NANO LETTERS

Letter

pubs.acs.org/NanoLett

Surface Hydrogen Enables Subeutectic Vapor−Liquid−Solid Semiconductor Nanowire Growth

Saujan V. Sivaram,[†] Ho Yee Hui,[†] María de la Mata,[‡] Jordi Arbiol,[‡,§] and Michael A. Filler*[,†]

[†]School of Chemical & Biomolecular Engineering, Georgia Institute of Technology, Atlanta, Georgia 30332, United States

[‡]Catalan Institute of Nanoscience and Nanotechnology (ICN2), CSIC and The Barcelona Institute of Science and Technology, Campus UAB, Bellaterra, Barcelona, Catalonia 08193, Spain

[§]Institució Catalana de Recerca i Estudis Avançats (ICREA), Barcelona, Catalonia 08010, Spain

Supporting Information

ABSTRACT: Vapor−liquid−solid nanowire growth below the bulk metal−semiconductor eutectic temperature is known for several systems; however, the fundamental processes that govern this behavior are poorly understood. Here, we show that hydrogen atoms adsorbed on the Ge nanowire sidewall enable AuGe catalyst supercooling and control Au transport. Our approach combines in situ infrared spectroscopy to directly and quantitatively determine hydrogen atom coverage with a "regrowth" step that allows catalyst phase to be determined with ex situ electron microscopy. Maintenance of a supercooled catalyst with only hydrogen radical delivery confirms the centrality of sidewall chemistry. This work underscores the importance of the nanowire sidewall and its chemistry on catalyst state, identifies new methods to regulate catalyst composition, and provides synthetic strategies for subeutectic growth in other nanowire systems.

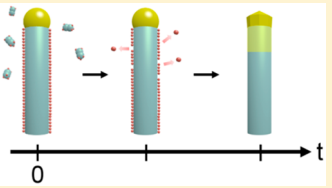

KEYWORDS: *semiconductor nanowire, vapor−liquid−solid mechanism, hydrogen, germanium*

The "bottom-up" vapor−liquid−solid (VLS) mechanism is a versatile method for semiconductor nanowire synthesis. The ability to encode different crystal structures,[1,2] alloy compositions,[3] dopant concentrations,[4] isotope distributions,[5] or heterostructures[6] along the nanowire length is a key benefit of VLS synthesis and can allow individual nanowires to function as complete devices.[7−9] A liquid eutectic catalyst droplet sitting atop the nanowire is central to the VLS growth mode. It acts as a reservoir for atomic species and directs nanowire crystallization.[10] The physicochemical factors that control catalyst phase, composition, and size—collectively referred to as the catalyst's "state"—must be understood to ab initio choreograph synthesis and control nanowire structure.

Catalyst state depends on, in addition to temperature, the relative rates of semiconductor (e.g., Si, Ge), metal (e.g., Au), and dopant (e.g., P, B) atom transport across the vapor−liquid, vapor−solid, and liquid−solid interfaces.[11] Two transport pathways are commonly considered when rationalizing nanowire growth: (1) delivery of atomic species into the catalyst through the vapor−liquid interface and (2) transport of atomic species from the catalyst to the nanowire via nucleation at the liquid−solid interface. However, catalyst state can also be influenced by the transport of species (3) to the gas phase through the vapor−liquid interface, (4) to the catalyst via dissolution at the liquid−solid interface, and (5) to/from the catalyst via surface diffusion along the vapor−solid interface. Recent work, by our group and others, indicates that pathways 3 and 4 can play an important role.[11−15] Reports of Au diffusion on the nanowire sidewall confirm that pathway 5 is not always negligible,[16−18] but the understanding of this pathway remains very limited.

In this Letter, we directly and quantitatively show how vapor−solid interface chemistry not only governs subeutectic VLS growth but also controls atomic transport between the catalyst and the sidewall. Subeutectic nanowire growth, where the catalyst remains liquid below the bulk metal−semiconductor eutectic temperature, has been suspected[19−23] and confirmed[24−26] for several systems, including Au−Ge, Al−Si, and Au−InAs. The present work shows that hydrogen atoms adsorbed on the sidewall block the transport of atomic species from the catalyst and, in doing so, prevent catalyst solidification. We unambiguously demonstrate this effect by delivering atomic hydrogen to the nanowire sidewall which preserves a liquid catalyst even in the absence of Ge_2H_6 flow. The catalyst solidification observed here is the source of the growth destabilization we previously reported.[27]

A three-step experimental procedure allows us to investigate the impact of sidewall hydrogen coverage on catalyst phase. Each of the three steps—"growth", "H_2 anneal", and "regrowth"—are outlined here, illustrated in Figure 1, and described in detail below. Following a combination of ex situ and in situ cleaning of a Ge(111) substrate,[27] a thin layer (∼1 nm) of Au is thermally evaporated onto the bare substrate. Vertical, untapered Ge nanowires with hydrogen-terminated sidewalls are synthesized in an initial "growth" step similar to that used previously.[27] After growth of a short Ge base, the majority of the nanowire is elongated for 60 min at 260 °C with

Received: April 21, 2016
Revised: June 8, 2016

DOI: 10.1021/acs.nanolett.6b01640
Nano Lett. XXXX, XXX, XXX−XXX

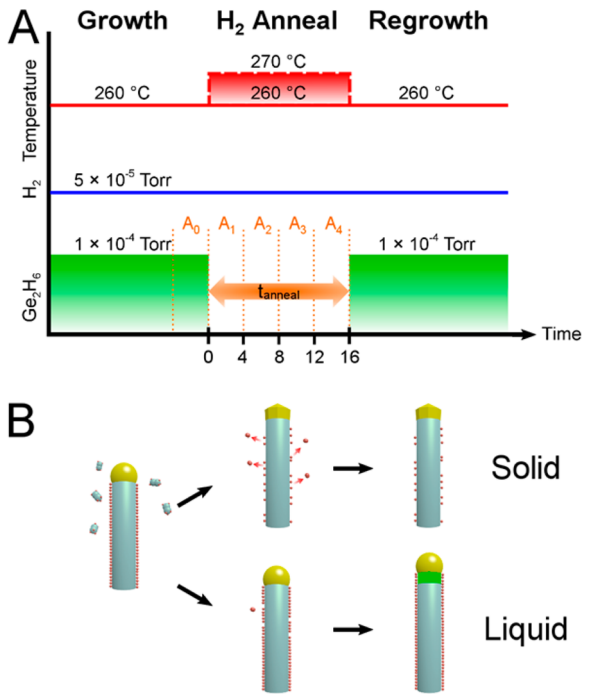

Figure 1. Procedure to determine catalyst phase. (A) Schematic plot of substrate temperature (T_{sub}), H_2 partial pressure, and Ge_2H_6 partial pressure versus time during the three step procedure. Ge_2H_6 is evacuated from the growth chamber during the "H_2 anneal" step and reintroduced during "regrowth." The value of t_{anneal} is variable. The orange dotted lines indicate the time intervals over which in situ infrared spectra are acquired. (B) Schematic showing catalyst droplets that remain liquid elongate via the subeutectic VLS mechanism when re-exposed to Ge_2H_6 during the regrowth step, whereas droplets that have solidified do not grow. Light blue represents the Ge nanowire and green corresponds to the nanowire segment grown after reintroduction of Ge_2H_6. The AuGe catalyst is shaded in gold and the red spheres represent hydrogen atoms.

Ge_2H_6 and H_2 partial pressures of 1×10^{-4} and 5×10^{-5} Torr, respectively. The "H_2 anneal" step begins by terminating Ge_2H_6 flow while holding the substrate temperature at 260 or 270 °C (T_{sub}) for a total time (t_{anneal}). Multiple growth runs are performed, each with a different anneal time (t_{anneal} = 4, 8, 12, or 16 min). We use in situ infrared spectroscopy during the H_2 anneal step to monitor the coverage of hydrogen atoms on the sidewall,[27] which decreases due to recombinative desorption as H_2. The value of t_{anneal} in any given experiment determines the number of absorption spectra recorded. For example, when t_{anneal} = 4 min, we acquire a single spectrum (A_1), whereas four spectra are recorded ($A_1 - A_4$) for t_{anneal} = 16 min. The final "regrowth" step is completed at T_{sub} = 260 °C for 8 min with Ge_2H_6 and H_2 partial pressures of 1×10^{-4} and 5×10^{-5} Torr, respectively (i.e., identical to the growth step). Catalysts that remain liquid after the H_2 anneal elongate further via the VLS mechanism when exposed to Ge_2H_6 again, whereas those that have solidified do not (Supporting Information, Figure S1). Enhanced sidewall roughening serves as a marker for the position of the catalyst–nanowire interface at the end of the H_2 anneal step (Supporting Information, Figure S2). This roughening allows us to assess regrowth for individual nanowires, and therefore determine the fraction of catalysts that remain liquid (f_{liquid}), with ex situ scanning electron microscopy (SEM). For catalysts that remain liquid, we find no difference in growth rates (~13 nm/min) between segments synthesized during the growth and regrowth steps. Solid catalysts may still be growing via the vapor–solid–solid (VSS) mechanism; however, the order of magnitude difference between VLS and VSS growth rates[24] along with the long regrowth time allow us to easily identify catalyst solidification. We attribute the kinked appearance of nanowires with solid catalysts to the rapid expulsion of Ge atoms from the AuGe catalyst, as seen in previous studies.[24]

The fraction of catalysts that remain liquid (f_{liquid}) decreases as the duration of the H_2 anneal step (t_{anneal}) increases. Figure 2A shows ex situ SEM images of nanowires annealed at T_{sub} =

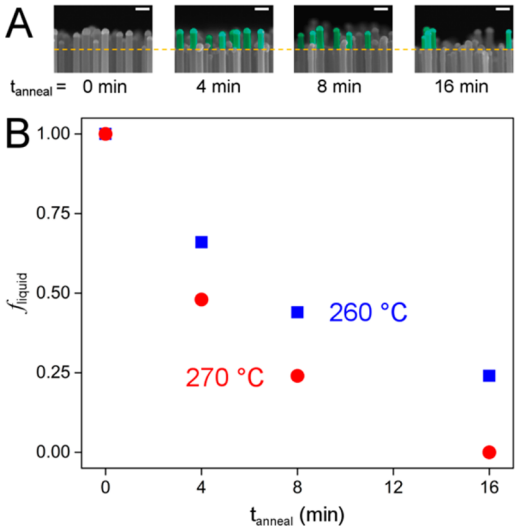

Figure 2. Catalyst state governed by H_2 anneal time and substrate temperature. (A) Representative postgrowth SEM images of nanowires after the regrowth step, with the newly elongated section false colored in green, as a function of total anneal time (t_{anneal}) at T_{sub} = 260 °C. The dashed line denotes the point where regrowth began. Scale bar, 100 nm. (B) Fraction of catalysts that remain liquid as a function of t_{anneal} and T_{sub}. N = 50 at each condition.

260 °C. As expected, all nanowires regrow when t_{anneal} = 0 min (i.e., continuous elongation). One can clearly see that as t_{anneal} increases, fewer nanowires elongate during the regrowth step. Figure 2B quantifies f_{liquid} as a function of H_2 anneal time. A similar trend is observed for nanowires annealed at T_{sub} = 270 °C; however, the rate of catalyst solidification is faster at 270 °C, such that no nanowires regrow beyond t_{anneal} = 16 min.

We also interrogate the coverage of hydrogen atoms on the nanowire sidewall during the H_2 anneal step with in situ infrared spectroscopy. Figure 3A,B shows a series of time-averaged absorption spectra, labeled A_n (where n = 0–4), for T_{sub} = 260 and 270 °C, respectively, and different values of t_{anneal}. As illustrated by the orange dotted lines in Figure 1A, the A_0 spectrum is the result of integrating 1000 individual scans over the last 4 min of the growth step. The A_1–A_4 spectra are acquired in the same manner over sequential 4 min intervals during the H_2 anneal step. Recall that the value of t_{anneal} dictates the maximum value of n for each experiment. The two absorption bands observed in each A_0 spectrum correspond to monohydride covalently bonded to the nanowire sidewall and are consistent with our previous work and other surface science studies.[27−29] The intensity of these ν(Ge–H) peaks decreases in each subsequently acquired spectrum (i.e., as n increases). Because the ν(Ge–H) integrated intensity is linearly proportional to the number of adsorbed hydrogen atoms,[27] we can

DOI: 10.1021/acs.nanolett.6b01640
Nano Lett. XXXX, XXX, XXX–XXX

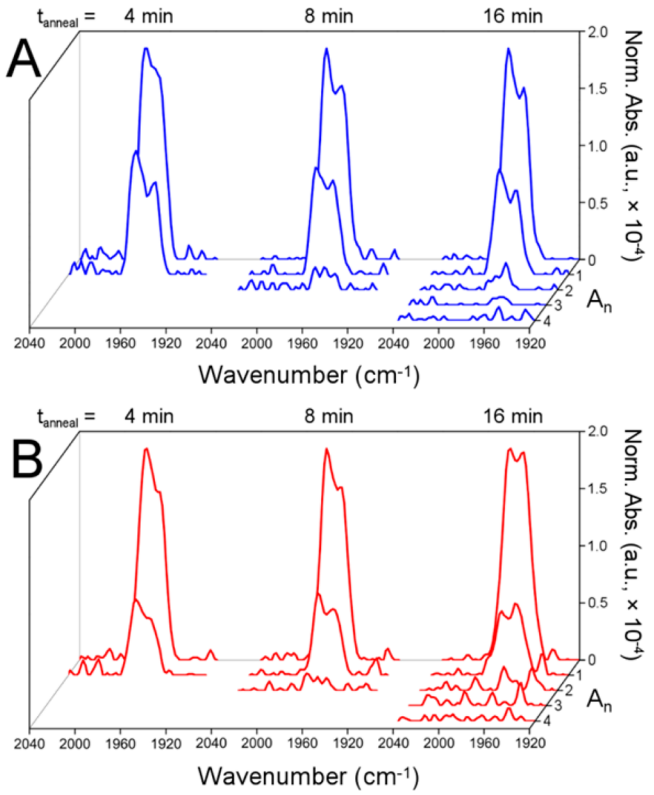

Figure 3. Loss of sidewall hydrogen during H_2 anneal. Time-averaged in situ infrared absorption spectra (A_n) of the ν(Ge−H) stretching region during the H_2 anneal step at T_{sub} = (A) 260 °C and (B) = 270 °C at different total H_2 anneal times (t_{anneal}). Each spectrum is comprised of 1000 individual scans recorded over 4 min. Spectrum A_0 is recorded during the final 4 min of the initial "growth" step (i.e., during Ge_2H_6 flow). Spectra A_1 through A_4 are recorded sequentially during the "H_2 anneal" step (i.e., after terminating Ge_2H_6 flow). Background spectra are of the Au-covered Ge(111) substrate maintained at the corresponding T_{sub} in vacuum.

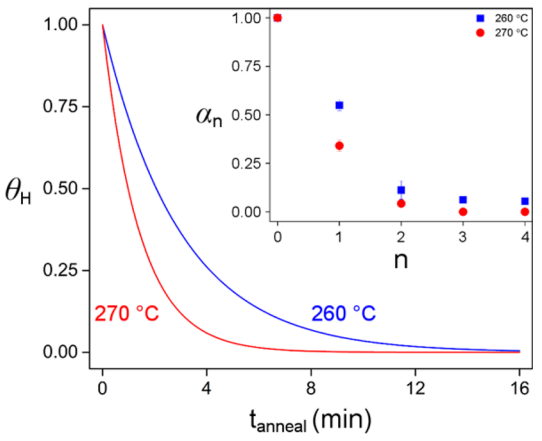

Figure 4. Determining sidewall hydrogen coverage as a function of time during the H_2 anneal step. Hydrogen coverage (θ_H) extracted from eq 2 and plotted as a function of time during the H_2 anneal at T_{sub} = 260 and 270 °C. Inset: Time-averaged hydrogen coverage (α_n) determined from eq 1 as a function of the spectrum number (n) at T_{sub} = 260 and 270 °C.

conclude that hydrogen atoms are recombinatively desorbing from the nanowire sidewall during the H_2 anneal (as H_2). Notably, hydrogen loss occurs despite maintaining a background pressure of H_2, which indicates that molecular H_2 has little impact on sidewall chemistry at these temperatures.

We can quantitatively determine the sidewall coverage of hydrogen atoms (θ_H)—the ratio of hydrogen-covered sidewall sites to total sites—as a function of time during the H_2 anneal step. We use the time-averaged absorption spectra (A_0–A_4) to calculate the time-averaged value of hydrogen atom coverage, α_n, via eq 1

$$\alpha_n = \frac{I_n}{I_0} = \frac{\int A_n(\tilde{\nu})\mathrm{d}\tilde{\nu}}{\int A_0(\tilde{\nu})\mathrm{d}\tilde{\nu}} \quad (1)$$

where I_n is the integrated ν(Ge−H) peak intensity determined from A_n, I_0 is the integrated ν(Ge−H) peak intensity determined from A_0, and $\tilde{\nu}$ is frequency in wavenumber. The Figure 4 inset shows that α_n decreases as n increases, as expected from the loss of ν(Ge−H) peak intensity seen in Figure 3.

We require an additional conversion to obtain a value of θ_H at any point in time during the H_2 anneal. Due to the time-averaged nature of our infrared measurements, the value of θ_H is higher at the beginning of any 4 min spectrum acquisition than at the end. We can extract θ_H by relating it to α_n with eq 2:

$$\alpha_n = \frac{1}{\Delta t}\int_t^{t+\Delta t} \theta_{H,o} e^{-kt} dt \quad (2)$$

where k is the Arrhenius rate constant for H_2 desorption, $\theta_{H,o}$ is the initial hydrogen coverage, and t is time. This equation assumes that the rate of hydrogen desorption is first order with respect to θ_H, which is appropriate for situations where surface diffusion is rapid and θ_H > 0.1.[30] Consistent with our prior work,[27] the initial hydrogen coverage is taken to be unity at the beginning of the H_2 anneal step (i.e., $\theta_{H,0}$ = 1 at t_{anneal} = 0 min). The value of k at T_{sub} = 260 and 270 °C is calculated from α_1. Figure 4 shows the resulting curve for θ_H as a function of time at any point during the H_2 anneal. We find good agreement between the time-averaged hydrogen coverage as measured directly with in situ infrared spectroscopy and that predicted from the curves in Figure 4 (Supporting Information, Table S1).

Figure 5 reveals a strong correlation between the fraction of catalysts that remain liquid (f_{liquid}) and the coverage of sidewall hydrogen (θ_H). The fact that the data points lie on a single curve for both H_2 anneal temperatures supports the hypothesis that hydrogen desorption leads to solidification. Notably, the relationship between f_{liquid} and θ_H is nonlinear. Approximately 25% of the catalysts remain liquid for the nanowire array held at T_{sub} = 260 °C for t_{anneal} = 16 min (Figure 2B), although the nanowire sidewall is nearly devoid of hydrogen (Figure 4). This behavior suggests that catalyst solidification is multistep process, but is ultimately regulated by nanowire surface chemistry.

We demonstrate that sidewall hydrogen enables the supercooled AuGe state by delivering atomic hydrogen (by cracking H_2 on a hot filament) during the H_2 anneal. The reactive hydrogen atom flux artificially maintains θ_H at a value higher than that possible at the same temperature with H_2 alone. Figure 6A shows that >90% of the catalysts remain liquid during such a H + H_2 anneal at T_{sub} = 260 °C for t_{anneal} = 16 min. As expected from the preceding discussion and observed in Figure 6B, the large majority of catalysts solidify during an H_2 anneal for t_{anneal} = 16 min at the same temperature and H_2

DOI: 10.1021/acs.nanolett.6b01640
Nano Lett. XXXX, XXX, XXX−XXX

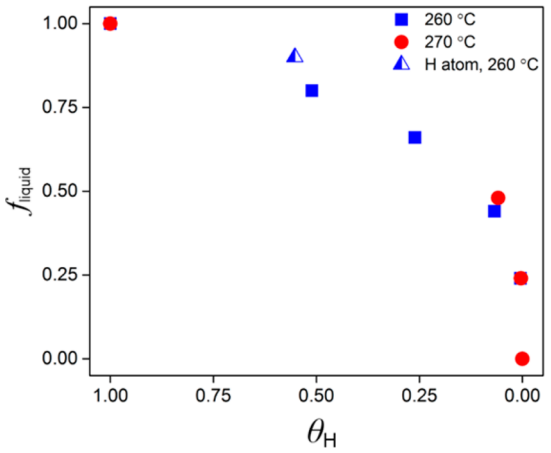

Figure 5. Connection of sidewall hydrogen and catalyst phase. Fraction of catalysts in supercooled AuGe state (f_{liquid}) as a function of θ_H and substrate temperature (T_{sub}). The "H atom" data point is from the H + H_2 anneal experiments shown in Figure 6.

partial pressure. In situ infrared absorption spectra recorded during H + H_2 annealing are shown in Figure 6C. Figure 6D shows that α_n reaches a steady-state value (i.e., equivalent rates of hydrogen adsorption and desorption) of ∼0.55 after the second spectrum. This value represents the actual θ_H since it is constant with time. Importantly, the data point from this H + H_2 experiment falls on the curve in Figure 5, indicating that the correlation between f_{liquid} and θ_H is general and not chemistry specific. These data also make clear, because the Ge_2H_6 partial pressure is zero during the H + H_2 anneal, that precursor delivery is not required to maintain the catalyst in a supercooled state.

A detailed examination of the nanowire sidewall provides further insight into the connection between surface hydrogen and catalyst phase. Figure 7 shows ex situ high angle annular dark field scanning transmission electron microscopy (HAADF-STEM) images of representative nanowires following growth, H + H_2 anneal, and H_2 anneal steps. We observe a clean sidewall, devoid of Au, upon terminating after the initial growth step (Figure 6A). The nanowire sidewall following H + H_2 annealing is also Au-free (Figure 6B). However, upon annealing in molecular H_2, significant quantities of Au are found on the sidewall (Figure 6C,D). Taken together, these data reveal that surface hydrogen, derived from Ge_2H_6 decomposition during growth or H atom flux during the H + H_2 anneal, acts as a diffusion barrier to Au.

Our experiments, which provide a direct probe of nanowire surface chemistry, yield important mechanistic insight into catalyst droplet supercooling and atomic transport during nanowire growth. We show that hydrogen atoms adsorbed on the nanowire sidewall block the transport of Au atoms, and quite likely Ge atoms, out of the catalyst. As described above, the concentration of any species (e.g., semiconductor or dopant atoms) in the catalyst is most often considered in terms of the rate of that species' delivery from the gas phase as well as its rate of removal due to nucleation of the solid nanowire or evaporation back to the gas phase.[11,12,31] This picture is valid when hydrogen atoms, or other adsorbed species (e.g., methyl groups, Cl, etc.), decorate the sidewall and block transport to the sidewall. However, a reduction of sidewall adsorbate coverage (assuming the solid−vapor interface energy remains low enough to prevent catalyst depinning) allows for the

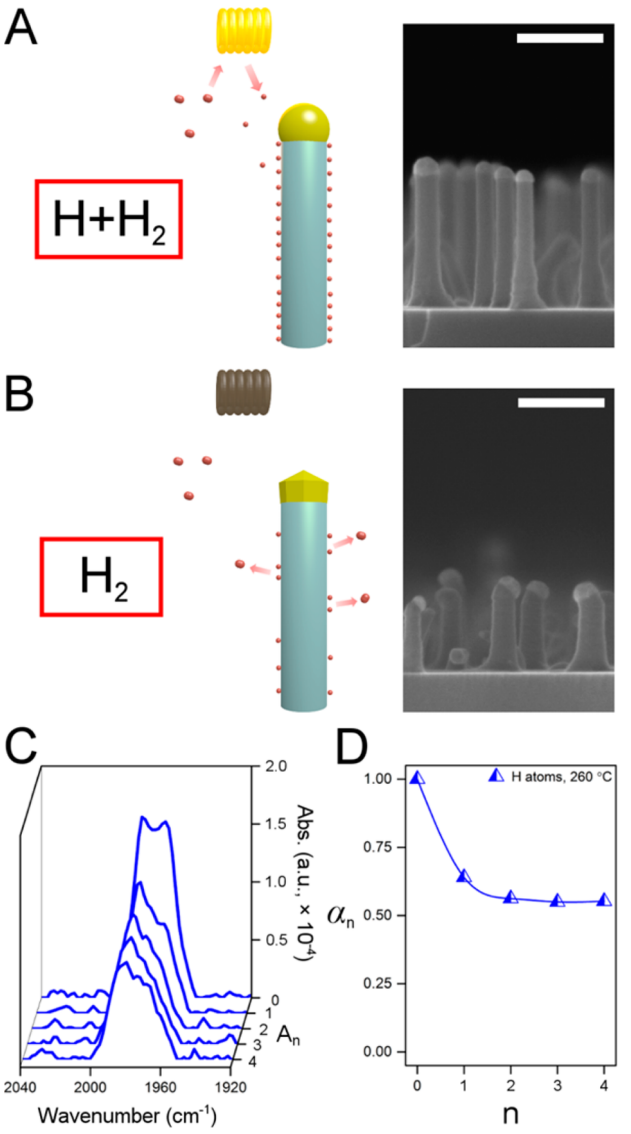

Figure 6. Atomic hydrogen preserves the supercooled AuGe state. (A) Schematic showing that H atoms, generated via cracking of H_2 at a hot tungsten filament (orange), can adsorb to the nanowire sidewall and maintain a liquid catalyst even in the absence of Ge_2H_6 flow. Representative postgrowth SEM image showing Ge nanowires exposed to H_2 + H atoms at T_{sub} = 260 °C for t_{anneal} = 16 min successfully elongate during regrowth. Scale bar, 100 nm. (B) Schematic showing molecular H_2 does not bind to the nanowire sidewall, leading to a net loss of sidewall hydrogen and subsequent catalyst solidification. Representative postgrowth SEM image shows Ge nanowires exposed to molecular H_2 at T_{sub} = 260 °C for t_{anneal} = 16 min do not elongate during regrowth. Scale bar, 100 nm. (C) Time-averaged in situ infrared absorption spectra of a nanowire array recorded during H_2 + H atom exposure at T_{sub} = 260 °C for t_{anneal} = 16 min. (D) Plot of time-averaged hydrogen coverage (α_n) as a function of spectrum number (n) during H_2 + H exposure. For large n, a steady-state hydrogen coverage is achieved and $\alpha_n = \theta_H$.

ejection of various species from the catalyst onto the sidewall. This pathway, whose activation threshold may be sidewall-adsorbate- and atomic-species-dependent, is likely to modify catalyst composition and influence nucleation. Differences in surface chemistry might, in fact, underlie the different droplet supersaturations observed for the Au/Si and Au/Ge systems (i.e., Au vs H terminated, respectively).[32,33] We also note that

DOI: 10.1021/acs.nanolett.6b01640
Nano Lett. XXXX, XXX, XXX−XXX

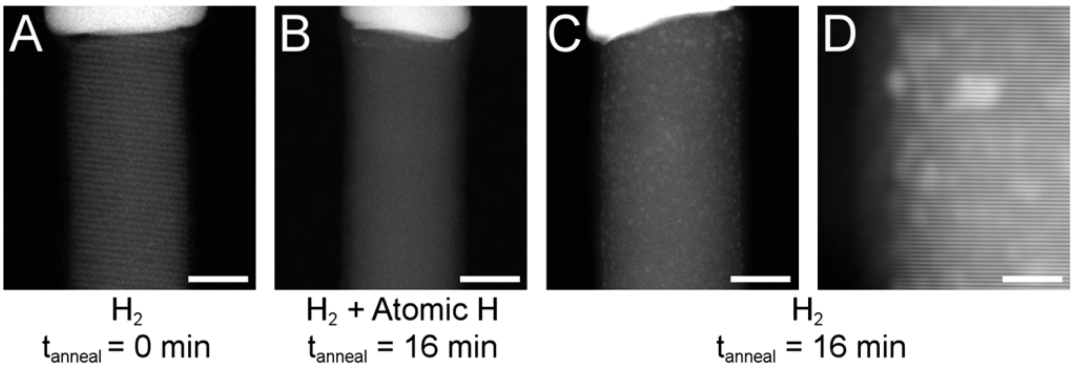

Figure 7. Sidewall hydrogen controls Au migration. HAADF-STEM images of representative Ge nanowires (A) immediately after the initial growth step showing no Au diffusion on the sidewall, (B) after an H + H_2 anneal at T_{sub} = 260 °C for t_{anneal} = 16 min also showing Au-free sidewalls, and (C) after an H_2 anneal at T_{sub} = 260 °C for t_{anneal} = 16 min exhibiting Au nanoparticles on the sidewall. Scale bars, 20 nm. (D) Magnified image of the nanowire sidewall after an H_2 anneal. Scale bar, 5 nm.

there is no reason to believe that the observed transport must always be *from the catalyst to the sidewall*.[34] Depending on the chemical potentials of different interfaces at different growth conditions, changes to the transport of species *from the sidewall to the catalyst* are also likely as surface coverage changes.

Sidewall hydrogen likely maintains AuGe catalysts in a supercooled state by (1) supporting a large Ge atom supersaturation and (2) preventing Au migration to the sidewall. Kodambaka et al. suggest that large Ge atom supersaturations yield a high barrier for Au nucleation.[24] Adsorbed hydrogen atoms likely create this situation by blocking Ge atom transport from the catalyst to the sidewall. The central importance of sidewall hydrogen, as opposed to Ge atom delivery,[24] to subeutectic growth in the Au/Ge system is supported by our H atom data (Figure 6). Surface hydrogen also blocks Au migration to the sidewall, preventing access to a low barrier nucleation site. Catalyst solidification, as observed here, can only occur after a sufficient loss of sidewall hydrogen. We do not observe a dependence of catalyst solidification on nanowire diameter (Supporting Information, Figure S3), which supports the argument that Au transport down the sidewall, rather than differences in catalyst supersaturation, controls the solidification process.

The fact that some catalysts remain liquid at small θ_H values (Figure 5) indicates that hydrogen desorption is only the initial step in the catalyst solidification process. We propose three major steps: (1) surface hydrogen desorption, (2) diffusion of Au atoms from the catalyst to the bare sidewall, and (3) Au nucleation. Additional studies are required to elucidate the relationship between Au diffusion to the sidewall and catalyst phase change. However, the variability of catalyst solidification time could result from a number of factors such as differences in local sidewall morphology or the inherent stochasticity of nucleation itself.[35]

In conclusion, we show that surface adsorbates can kinetically trap a nanowire catalyst droplet in a supercooled state. We anticipate that this mechanism, though specifically demonstrated here for the Au/Ge system, is active in other systems with sufficiently reactive precursors and large sidewall adsorbate coverages (e.g., Al/Si). We further show how surface adsorbates are critical arbiters of atomic transport between the catalyst droplet and the nanowire sidewall. Our experiments provide important insight into the influence of vapor phase composition and substrate temperature on nanowire sidewall chemistry, catalyst state, and ultimately structure and properties. They also motivate the development of designer precursors to better control these fundamental processes and, in doing so, advance doping,[8,36,37] crystal phase modulation,[38,39] and heterostructure formation.[6,40]

Methods: Substrate Preparation. Ge(111) substrates are prepared by the method previously described.[27] Briefly, double-side polished Ge(111) wafers (MTI Corp., CZ, 500 μm, 42−64 Ω·cm) are cleaved using a diamond scribe and chemically cleaned through repeated oxidation-etch cycles. An oxide layer is formed by immersion of the substrate into an aqueous 3 wt % H_2O_2 (JT Baker, 30 wt %, ACS grade) solution and then etched away in 9% HCl (JT Baker, CMOS grade). Between each step, the substrate is rinsed with copious amounts of deionized (DI) water and dried with N_2 gas (Airgas, 99.999%). A final oxide is formed by immersing the substrate in a solution of 1:2:20 NH_4OH:H_2O_2:H_2O. The sample is then rinsed and dried prior to loading into the ultrahigh vacuum (UHV) system. The substrate is first annealed at T_{sub} = 525 °C for 35 min to desorb the oxide layer. Substrate temperature is measured using a calibrated infrared pyrometer (Mikron). In situ cleaning is performed by exposure of the substrate to Ge_2H_6 (Voltaix, 20% in He) at T_{sub} = 305 °C. The quality of the substrate is assessed by the full width at half-maximum (fwhm) of the ν(Ge−H) peak at room temperature. Finally, the substrate is briefly heated to T_{sub} = 420 °C to desorb surface hydrogen from the in situ cleaning step and a thin layer of Au is evaporated in situ with a Knudsen cell (SVT Associates).

Nanowire Growth and Annealing Procedure. The UHV system where nanowire growth occurs has been described elsewhere.[27] The low base pressure of the chamber (3×10^{-10} Torr) minimizes the influence of gaseous contaminants during the synthesis. The nanowire "growth" step (Figure 1A) begins with the substrate oriented 58° relative to the infrared beam path and facing the Ge_2H_6 directed doser. Short Ge nanowire stubs are initially grown by heating from room temperature to T_{sub} = 420 °C in a Ge_2H_6 partial pressure of 2×10^{-6} Torr. After 30 s at T_{sub} = 420 °C, the substrate is cooled to T_{sub} = 305 °C at a rate of 2 °C/s. The Ge_2H_6 partial pressure is then increased to 1×10^{-4} Torr and held constant for 5 min, yielding 100 nm Ge nanowire stubs. The majority of the "growth" step consists of nanowire elongation, which is accomplished by cooling to T_{sub} = 260 °C, orienting the substrate perpendicular to the infrared beam path (i.e., 0°), and adding H_2 at a partial pressure of 5×10^{-5} Torr. The "H_2 anneal" step (Figure 1A) begins by closing the Ge_2H_6 leak

DOI: 10.1021/acs.nanolett.6b01640
Nano Lett. XXXX, XXX, XXX−XXX

valve, but maintaining H_2 flow. The temperature is either held at T_{sub} = 260 °C or raised to T_{sub} = 270 °C in 10 s. In each nanowire growth run, the "H_2 anneal" step is performed for a different time (t_{anneal}). The final "regrowth" step (Figure 1A) begins with the reintroduction of Ge_2H_6 at a partial pressure of 1×10^{-4} Torr at T_{sub} = 260 °C. For experiments with an "H_2 anneal" step at T_{sub} = 270 °C, the temperature is first decreased to T_{sub} = 260 °C in 5 s and Ge_2H_6 is then added to the chamber. "Regrowth" proceeds for 8 min after which the substrate is rapidly cooled in the Ge_2H_6 and H_2 background and the chamber is evacuated of gases.

In Situ Infrared Absorption Spectroscopy. A Fourier transform infrared (FTIR) spectrometer (Bruker, Vertex 70) equipped with a narrowband liquid N_2-cooled HgCdTe (MCT) detector is coupled to the vacuum chamber and used to measure the vibrational modes of surface adsorbates.[27] All measurements are recorded in situ under the conditions shown in Figure 1A, utilizing unpolarized light and a spectrometer resolution of 4 cm^{-1}. Each spectrum consists of 1000 scans and is referenced to the Au-covered Ge(111) surface heated to T_{sub} = 260 or 270 °C. As described in the main text, spectrum A_0 is collected over the last 4 min of the "growth" step, whereas spectra A_1 through A_4 are collected sequentially during the "H_2 anneal" step. All spectra are baseline-corrected using a standard concave rubber band method.

Electron Microscopy. Nanowire morphology is examined with a Zeiss Ultra60 field emission scanning electron microscope (SEM). Transmission electron microscopy (TEM) images are collected with a probe-corrected FEI Titan 60−300 microscope operated at 300 keV, providing a lateral resolution below 0.1 nm.

■ ASSOCIATED CONTENT

Supporting Information

The Supporting Information is available free of charge on the ACS Publications website at DOI: 10.1021/acs.nanolett.6b01640.

SEM images, number of liquid and solid catalysts, comparison of the time-averaged hydrogen coverage. (PDF)

■ AUTHOR INFORMATION

Corresponding Author

*E-mail: mfiller@gatech.edu.

Author Contributions

S.V.S. and H.Y.H. collected the in situ infrared spectroscopy and SEM data. S.V.S. and M.A.F. jointly analyzed the data and wrote the manuscript. J.A. and M.d.l.M. collected and analyzed the TEM data. All authors approved the final version.

Notes

The authors declare no competing financial interest.

■ ACKNOWLEDGMENTS

M.A.F., S.V.S., and H.Y.H. gratefully acknowledge the financial support of the National Science Foundation (#1133563 and #1150755). S.V.S. and H.Y.H. also thank the NSF IGERT program (#1069138) and the Archibald McNeill Endowment at Georgia Tech, respectively, for additional support. The HAADF-STEM microscopy was conducted in the Laboratorio de Microscopias Avanzadas at the Instituto de Nanociencia de Aragon—Universidad de Zaragoza. J.A. and M.d.l.M. thank them for offering access to their instruments and expertise. Interactions with Dr. Jane Y. Howe were fruitful and appreciated.

■ REFERENCES

(1) Caroff, P.; Dick, K. A.; Johansson, J.; Messing, M. E.; Deppert, K.; Samuelson, L. *Nat. Nanotechnol.* **2009**, *4*, 50.

(2) Algra, R. E.; Verheijen, M. A.; Borgstrom, M. T.; Feiner, L. F.; Immink, G.; van Enckevort, W. J. P.; Vlieg, E.; Bakkers, E. *Nature* **2008**, *456*, 369.

(3) Kuykendall, T.; Ulrich, P.; Aloni, S.; Yang, P. *Nat. Mater.* **2007**, *6*, 951.

(4) Chou, L.-W.; Shin, N.; Sivaram, S. V.; Filler, M. A. *J. Am. Chem. Soc.* **2012**, *134*, 16155.

(5) Mukherjee, S.; Givan, U.; Senz, S.; Bergeron, A.; Francoeur, S.; de la Mata, M.; Arbiol, J.; Sekiguchi, T.; Itoh, K. M.; Isheim, D.; Seidman, D. N.; Moutanabbir, O. *Nano Lett.* **2015**, *15*, 3885.

(6) Wen, C. Y.; Reuter, M. C.; Bruley, J.; Tersoff, J.; Kodambaka, S.; Stach, E. A.; Ross, F. M. *Science* **2009**, *326*, 1247.

(7) Qing, Q.; Jiang, Z.; Xu, L.; Gao, R.; Mai, L.; Lieber, C. M. *Nat. Nanotechnol.* **2013**, *9*, 142.

(8) Wallentin, J.; Anttu, N.; Asoli, D.; Huffman, M.; Åberg, I.; Magnusson, M. H.; Siefer, G.; Fuss-Kailuweit, P.; Dimroth, F.; Witzigmann, B.; Xu, H. Q.; Samuelson, L.; Deppert, K.; Borgström, M. T. *Science* **2013**, *339*, 1057.

(9) Qian, F.; Gradečak, S.; Li, Y.; Wen, C.-Y.; Lieber, C. M. *Nano Lett.* **2005**, *5*, 2287.

(10) Schmidt, V.; Wittemann, J. V.; Gosele, U. *Chem. Rev.* **2010**, *110*, 361.

(11) Shakthivel, D.; Raghavan, S. *J. Appl. Phys.* **2012**, *112*, 024317.

(12) Pinion, C. W.; Nenon, D. P.; Christesen, J. D.; Cahoon, J. F. *ACS Nano* **2014**, *8*, 6081.

(13) Hui, H. Y.; Filler, M. A. *Nano Lett.* **2015**, *15*, 6939.

(14) Hudak, B. M.; Chang, Y.-J.; Yu, L.; Li, G.; Edwards, D. N.; Guiton, B. S. *ACS Nano* **2014**, *8*, 5441.

(15) Pennington, R. S.; Jinschek, J. R.; Wagner, J. B.; Boothroyd, C. B.; Dunin-Borkowski, R. E. *Journal of Physics: Conference Series* **2010**, *209*, 012013.

(16) Hannon, J. B.; Kodambaka, S.; Ross, F. M.; Tromp, R. M. *Nature* **2006**, *440*, 69.

(17) Dayeh, S. A.; Mack, N. H.; Huang, J. Y.; Picraux, S. T. *Appl. Phys. Lett.* **2011**, *99*, 023102.

(18) Luo, Z.; Jiang, Y.; Myers, B. D.; Isheim, D.; Wu, J.; Zimmerman, J. F.; Wang, Z.; Li, Q.; Wang, Y.; Chen, X.; Dravid, V. P.; Seidman, D. N.; Tian, B. *Science* **2015**, *348*, 1451.

(19) Moutanabbir, O.; Senz, S.; Scholz, R.; Alexe, M.; Kim, Y.; Pippel, E.; Wang, Y.; Wiethoff, C.; Nabbefeld, T.; Meyer zu Heringdorf, F.; Horn-von Hoegen, M. *ACS Nano* **2011**, *5*, 1313.

(20) Noor Mohammad, S. *J. Chem. Phys.* **2009**, *131*, 224702.

(21) Adhikari, H.; Marshall, A. F.; Goldthorpe, I. A.; Chidsey, C. E. D.; McIntyre, P. C. *ACS Nano* **2007**, *1*, 415.

(22) Wacaser, B. A.; Reuter, M. C.; Khayyat, M. M.; Wen, C. Y.; Haight, R.; Guha, S.; Ross, F. M. *Nano Lett.* **2009**, *9*, 3296.

(23) Tchernycheva, M.; Travers, L.; Patriarche, G.; Glas, F.; Harmand, J.-C.; Cirlin, G. E.; Dubrovskii, V. G. *J. Appl. Phys.* **2007**, *102*, 094313.

(24) Kodambaka, S.; Tersoff, J.; Reuter, M. C.; Ross, F. M. *Science* **2007**, *316*, 729.

(25) Gamalski, A. D.; Tersoff, J.; Sharma, R.; Ducati, C.; Hofmann, S. *Nano Lett.* **2010**, *10*, 2972.

(26) Gamalski, A. D.; Ducati, C.; Hofmann, S. *J. Phys. Chem. C* **2011**, *115*, 4413.

(27) Sivaram, S. V.; Shin, N.; Chou, L.-W.; Filler, M. A. *J. Am. Chem. Soc.* **2015**, *137*, 9861.

(28) Lu, G. Q.; Crowell, J. E. *J. Chem. Phys.* **1993**, *98*, 3415.

(29) Chabal, Y. J. *Surf. Sci.* **1986**, *168*, 594.

(30) Lee, J. Y.; Maeng, J. Y.; Kim, A.; Cho, Y. E.; Kim, S. *J. Chem. Phys.* **2003**, *118*, 1929.

(31) Christesen, J. D.; Pinion, C. W.; Zhang, X.; McBride, J. R.; Cahoon, J. F. *ACS Nano* **2014**, *8*, 11790.

DOI: 10.1021/acs.nanolett.6b01640
Nano Lett. XXXX, XXX, XXX−XXX

(32) Kim, B. J.; Tersoff, J.; Kodambaka, S.; Reuter, M. C.; Stach, E. A.; Ross, F. M. *Science* **2008**, *322*, 1070.
(33) Kim, B. J.; Wen, C. Y.; Tersoff, J.; Reuter, M. C.; Stach, E. A.; Ross, F. M. *Nano Lett.* **2012**, *12*, 5867.
(34) Dubrovskii, V. G.; Sibirev, N. V.; Harmand, J. C.; Glas, F. *Phys. Rev. B: Condens. Matter Mater. Phys.* **2008**, *78*, 235301.
(35) Leonard, J. P.; Im, J. S. *Appl. Phys. Lett.* **2001**, *78*, 3454.
(36) Perea, D. E.; Hemesath, E. R.; Schwalbach, E. J.; Lensch-Falk, J. L.; Voorhees, P. W.; Lauhon, L. J. *Nat. Nanotechnol.* **2009**, *4*, 315.
(37) Kempa, T. J.; Tian, B. Z.; Kim, D. R.; Hu, J. S.; Zheng, X. L.; Lieber, C. M. *Nano Lett.* **2008**, *8*, 3456.
(38) Assali, S.; Gagliano, L.; Oliveira, D. S.; Verheijen, M. A.; Plissard, S. R.; Feiner, L. F.; Bakkers, E. P. A. M. *Nano Lett.* **2015**, *15*, 8062.
(39) Jacobsson, D.; Panciera, F.; Tersoff, J.; Reuter, M. C.; Lehmann, S.; Hofmann, S.; Dick, K. A.; Ross, F. M. *Nature* **2016**, *531*, 317.
(40) Hillerich, K.; Dick, K. A.; Wen, C.-Y.; Reuter, M. C.; Kodambaka, S.; Ross, F. M. *Nano Lett.* **2013**, *13*, 903.

DOI: 10.1021/acs.nanolett.6b01640
Nano Lett. XXXX, XXX, XXX−XXX